Article:
Wang, H, Khodaparast, S, Carroll, J et al. (2020) A microfluidic-multiwell platform for rapid phase mapping of surfactant solutions. Review of Scientific Instruments, 91 (4). 045109. ISSN: 0034-6748

https://doi.org/10.1063/1.5144770

A Microfluidic-Multiwell Platform for Rapid Phase Mapping of Surfactant Solutions

Haoyu Wang,[1, a)] Sepideh Khodaparast,[1] John Carroll,[2] Caroline Kelly,[2] Eric S. J. Robles,[3] and João T. Cabral[1, b)]
[1)]*Department of Chemical Engineering, Imperial College London, London SW7 2AZ, U.K.*
[2)]*National Formulation Centre, Centre for Process Innovation, Sedgefield DL1 1GL, U.K.*
[3)]*Procter & Gamble, Newcastle Innovation Centre, Newcastle-Upon-Tyne NE12 9TS, U.K.*

(Dated: 30 March 2020)

Measurement of the phase behaviour and (meta)stability of liquid formulations, including surfactant solutions, is required for the understanding of mixture thermodynamics, as well as their practical utilisation. We report a microfluidic platform with a stepped temperature profile, imposed by a dual Peltier module, connected to an automated multiwell plate injector and optical setup, for rapid solution phase mapping. The measurement protocol is defined by the temperature step $\Delta T \equiv T_1 - T_2$ ($\lesssim 100$ °C), volumetric flow rate $Q \equiv \Delta V/\Delta t$ ($\lesssim 50$ μL/min) which implicitly set the thermal gradient $\Delta T/\Delta t$ ($\simeq$0.1–50°C/min), and measurement time (which must exceed the intrinsic timescale of the relevant phase transformation). Further, U-shaped microchannels can assess the reversibility of such transformation, yielding a facile measurement of the metastable zone width (MSZW) of the phase diagram. By contrast with traditional approaches, the platform precisely controls the cooling and heating rates by tuning flow rate, and the absolute temperature excursion by the hot and cold thermal profile, which remain stationary during operation, thus allowing the sequential and reproducible screening of large sample arrays. As a model system, we examine the transition from the micellar (L_1) to the liquid crystalline lamellar phase (L_α), upon cooling, of aqueous solutions of Linear Sodium Alkylbenzene Sulfonate (NaLAS), a biodegradable anionic surfactant extensively employed in industry. Our findings are validated with quiescent optical microscopy and Small Angle Neutron Scattering (SANS) data.

I. INTRODUCTION

Liquid 'formulations' are ubiquitous in personal and home care, oil and lubricants, foods, coatings, agri-chemical and pharmaceutical industries,[1–6] and generally comprise several components (surfactants, polymers, colloids, etc.) exhibiting complex phase behavior and metastability. Mapping the phase behaviour of such mixtures is intrinsically challenging due to their large parameter space, and the variety of so-called 'failure modes' which can include demixing, precipitation, crystallisation, gelation etc. Conventional measurement methods of temperature-composition phase boundaries generally rely on imposing a temperature change of a sample solution of prescribed composition at a constant cooling or heating rate ($\Delta T/\Delta t$) and on the detection of the relevant phase change through optical (e.g. turbidimetry, scattering, microscopy), illustrated in Fig. 1, or rheo-mechanical methods.

The rate-dependence of phase changes, as well as the large compositional parameter space, renders conventional methods rather challenging for formulations, requiring long experimental times. A single concentration is typically measured at several cooling/heating rates since these impact the apparent detection of phase change, and a temperature-rate extrapolation is normally required to approximate the thermodynamic boundaries, e.g. liquid-liquid demixing, to a 'zero' rate. In the context of crystallisation, for instance, the difference between the apparent phase boundaries detected upon cooling and heating at a *fixed rate* defines the so-called Metastable Zone Width (MSZW), between the solubility line curve and the metastability limit (or the saturation temperature and crystal detection temperature). This offset and the MSZW are illustrated in Fig. 1(b-c), and is strongly influenced by rate, requiring a series of experiments for its rigorous determination.

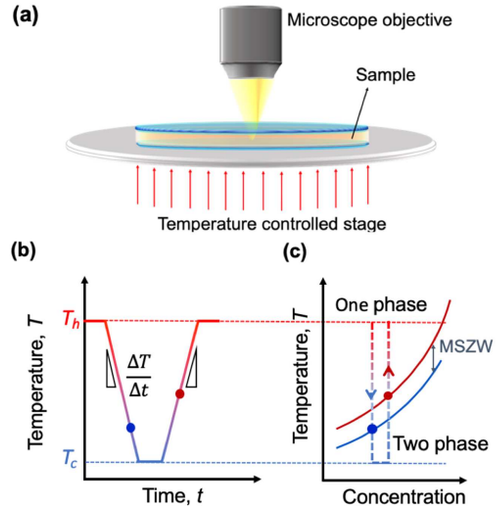

FIG. 1. (a) Schematic of conventional optical measurement of the phase diagram of a formulation, e.g. a surfactant solution cooled between glass slides over a thermal stage and under reflection optical microscopy. (b) Schematic of a temperature profile imposing prescribed cooling and heating rates ($\frac{\Delta T}{\Delta t}$) and the detection of the apparent phase boundaries, yielding a determination of a (c) Metastable Zone Width (MSZW), as the thermal width corresponding to the phase change (e.g. crystallisation) which is rate-dependent.

In order to screen multiple mixtures of diverse composition simultaneously, mutil-well plates and readers are often em-

[a)]Electronic mail: haoyu.wang@imperial.ac.uk
[b)]Electronic mail: j.cabral@imperial.ac.uk

ployed in an industrial or high-throughput context. To miniaturize sample volumes, 6 to 96-well (up to 384 or 1536-well) plates, with increasing sample density and decreasing volume (from ∼2 mL to 12.5 μL), and robotic liquid handlers, are often employed. A variety of plate readers employing assays including optical, spectroscopic and scattering probes have been developed, and can be subjected to a temperature controlled environment to estimate phase boundaries. The use of microarrays has been demonstrated[7] to investigate the phase behaviour of polymer solutions of various composition under uniform cooling conditions. While these approaches are clearly attractive for large sample libraries, as those relevant in formulation screening, such systems are generally expensive, often susceptible to sample evaporation, and can impose relatively slow temperature changes and limited thermal profiles.[8–11] A number of analytical solutions[12] are commercially available, seeking to 'accelerate' formulation stability testing (e.g. under temperature storage or freeze-thaw-cycles) to assess phase behaviour or metastability (in terms of a 'shelf-life') under expected conditions of storage or usage. These include inclination and analytical centrifugation,[13] multiple light scattering profiling,[14] automated sample changing for rheology, or calorimetry, or other conventional analytical probes, such as spectroscopy[15], ultrasound,[16] and electrical conductivity.[17]

Microfluidics. The advent of microfluidics[18,19] has opened a range of new possibilities for the handling, processing and testing of complex fluid formulations. Microfluidics has been employed to generate (static) arrays of droplets of prescribed composition, enabling phase diagram measurements by imposing static (but spatially-varying) or time-varying (spatially uniform) temperature fields. Shangguan et al.[20] reported the phase mapping of polymer solutions upon cooling of a series of solution droplets of different concentrations stored in a glass capillary with laser light scattering. Laval et al.[21] applied a temperature gradient to a microchip with parallel channels for the screening of solubility diagrams. The droplet composition was same in each channel but varied in different channels such that, by imposing a temperature gradient along the channels, the phase boundary could be detected within the microchip. Several microfluidic platforms (often fabricated in polydimethylsiloxane, PDMS) have been exploited to study the phase behaviour of complex mixtures,[22,23] exploiting droplet microfluidics and evaporation or water permeation in PDMS for selected aqueous systems. In this context, static or 'gentle' flow conditions are employed to eliminate flow-induced perturbations,[24–28] to otherwise quiescent phase behavior measurements. In the field of molecular biology, temperature cycling in microfluidics has been implemented to carry out polymerase chain reactions (PCR) for high efficiency DNA amplification with minute sample volumes.[29,30]

A novel microfluidic platform and model system. Inspired by advances in microfluidics and PCR, here we report an integrated microfluidic platform for rapid phase mapping of liquid formulations exposed to thermal gradients under flow. The system consists of a microfluidic device subjected to a thermal gradient along the flow direction, connected to a multiwell plate from which distinct compositions are convected sequentially and measured optically. The non-trivial features of our approach arise from the coupling between the flow velocity of sample plugs and the static temperature profile which (dynamically) defines the temperature ramp, and from the use of U-shaped microchannel designs capable of temperature cycling and a facile measurement of the MSZW in exceptionally controlled conditions. For this demonstration, we employ a micellar surfactant solution and map its phase behaviour as a function of concentration and temperature. We select a commercially significant, biodegradable, anionic surfactant, namely Sodium Linear Alkylbenzene Sulfonate (NaLAS)[31] for our study, and focus on the transition from the micellar phase (L_1) to the lamellar phase (L_α), forming multilamellar vesicles (MLV)[32] upon cooling. We evaluate the platform employing segmented flows of NaLAS/water mixtures and benchmark our rapid phase mapping and MSZW results with conventional optical microscopy and SANS data. Various potential modes of operation and their relative merits are then discussed.

II. DESIGN OF THE PLATFORM

The platform consists of a custom-designed (A) thermal stage, (B) microfluidic chip, (C) optical diagnostic setup, and (D) automated sampling unit, illustrated in Fig. 2. The microfluidic chip is placed atop the thermal stage and solutions of prescribed concentration are convected into the microdevice by withdrawal from a multiwell plate equipped with xyz displacement and a fine nozzle, using a syringe pump. Automated image analysis is carried out as various solution compositions are convected along the thermal gradient profile.

A. Thermal stage system

The thermal stage system is a customized dual Peltier module system developed in collaboration and fabricated by Linkam Scientific. The Peltier stages (4 cm ×4 cm, nickel coated) are arranged side by side, separated by an 8 mm gap, whose temperature can be individually computer-controlled within a temperature range of -40°C to 120°C, and 0.01°C precision. These are generally kept at fixed (but distinct) temperatures, which can be altered at a cooling/heating rate of up to 30°C/min. The system is fully enclosed and the top cover has a large transparent glass window (4 cm × 8 cm) which seals the stage while enabling optical imaging (or scattering). Lateral ports for microfluidic tubing (inlets and outlet) and purge gases are available.

B. Microdevices

The two microchips demonstrated in the current work, with straight or U-shaped channels, were lab-made using frontal photopolymerization (FPP)[33] of a thiolene resin (NOA81, Norland optics) with a photomask, between 1 mm-thick glass slides. The microchannels are 1000 μm wide and 400 μm

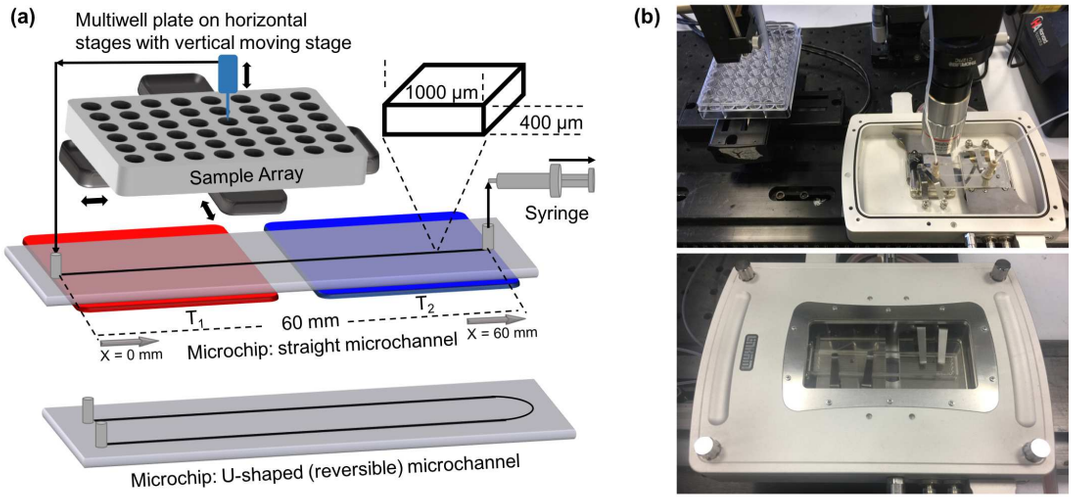

FIG. 2. (a) Schematic of the system including a multiwell plate mounted onto two horizontal (xy) moving stages and a microchip (straight and U-shaped microchannel) placed onto the dual temperature stage. A syringe continuously withdraws samples from the multiwell plate via a vertical (z) moving stage connected through the microchip. (b) Image of the open and enclosed setup, with optically transparent window for inspection in both transmission and reflection modes.

deep with length of 6 cm and 13 cm for the straight and U-shaped channels, respectively. A diamond tip drill bit was used to drill two holes on the top slide. The UV-curable resin was exposed for 90 s using a 365 nm UV Lamp (OmniCure S1500) at 5 mW/cm^2 intensity, yielding a dose of 0.45 J/cm^2. The unexposed liquid thiolene within the channel was removed by flushing with ethanol and (briefly) with acetone. The chip was then post cured for another 15 min at the same intensity. A nanoport (Upchurch N-333) was then attached to each hole with two-part liquid adhesive (Araldite Rapid), and connected to tubing PEF tubing (Cole-Parmer, o.d. 1/16 in., i.d. 1/32 in.) and to a high-pressure syringe pump (Harvard PHD Ultra 4400) via the metal syringe (Harvard 20 ml Stainless Steel Syringe with 1/16 inch SWAGELOK) on the outlet. The microchip is placed in conformal contact onto the polished Peltier stages, across the 8 mm gap, and clamped into position.

To characterise the thermal profile of the system, detailed measurements and numerical simulation of thermal profile across the microchannel were carried out and compared in Fig. 3. The surface temperature of the two Peltier elements was set to 40°C (hot side) and 0°C (cold side) and multiple thermocouples were bonded along the microchannel between the glass slides to assess the temperature gradient in depth (z) and in-plane (xy), over the thermal stages. The temperature profile was found to be flat toward the external boundaries of the hot and the cold stages and exhibit a sigmoidal profile between the two modules with a largely linear profile across the gap. Non-linear recessed regions can be observed near the edges of the Peltier elements, associated with the lateral heat conduction along the microchannel glass plates and plastic matrix. Simulations were carried out with the open source CFD software package, OpenFOAM, to calculate the temperature profile along the microchannel (in the presence and absence of flow) and compared with experiment, to enable the rapid computation of thermal profiles under various flow conditions. At these flow rates (1-15 μL/min), corresponding to average flow velocities of $v \simeq$40-600 μm/s, the flow induced thermal offset is modest, yielding equilibration times below $\simeq$1 s (estimated from $\Delta x_{offset}/v$ at 15μL/min).

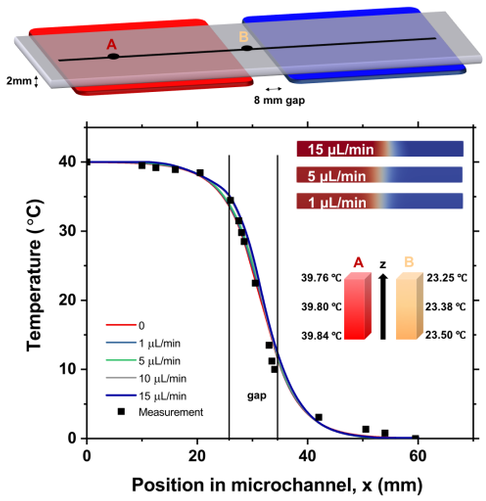

FIG. 3. Comparison of the numerical simulation (solid lines) at different flow rates (indicated) and experimental measurement (full squares, quiescent) of the temperature along the microchannel in the centre of the 1+1 mm thick glass microchip placed atop the thermal stages set to 40°C and 0°C. The position along the microchannel, x, is defined as the distance of the inlet, and the 8 mm gap is centred at position x=30 cm. The temperature profile of the microchannel at two points, A (on the top of thermal stage) and B (in the gap) at 5 μL/min across the height of the channel is illustrated in the subfigure. The temperature variance between the bottom (close to thermal source) and the top is less then 0.2°C.

C. Optical microscopy

A homemade tube reflecting microscope is used for optical detection, comprising a Mitutoyo M plan 5x long working distance objective, Mitutoyo to C-mount adapter, infinity corrected tube lens (Thorlabs, TTL165-A), a broadband beam splitter cube (Thorlabs, BS013), in-line LED light source (Thorlabs, M530,L3), and a digital camera (Basler acA2000-165um). The optical setup provided a spacial resolution of 1.4 μm per pixel. The microscope is mounted on an xyz manual linear translational stage (Thorlabs, XR25C).

D. Automated sampling unit

The sampling unit consists of a multiwell plate (Costar), xyz stages, and a syringe pump. For the demonstration here, standard 48 or 96 sample plates were employed, and mounted onto two orthogonal (xy) motorized linear translational stages (Thorlabs, DDSM100). A vertically moving (z-axis) motorized linear translational stage (Thorlabs, PT1-Z8) connected to a needle tubing assembly (1/16", length $\simeq$ 30 cm) is controlled by DC Servo Drivers (Thorlabs, KBD101) together with the xy stages via LabView using Thorlabs Kinesis® software. A Harvard PHD 2000 Advance syringe pump is used to continually withdraw liquid samples from the multiwell plate through the microchannel. At every step, the xy stage moves the multiwell plate such that the relevant sample well is placed under the aspiration assembly and the z-stage is then activated to dip the needle tubing and withdraw a prescribed volume of solution. Between each sample aspiration and xy-z displacement step, an air plug is introduced into the tubing, thus compartmentalizing each sample. As a result, a series of sample plugs are sequentially loaded into the microchip from the multiwell plate using a single syringe pump. This protocol can be trivially modified to include a 'wash' step between sample loading, as described below.

III. EXPERIMENTAL PROCEDURE

For the model system employed here, NaLAS/water micellar solutions at <30% mass fraction surfactant concentrations, the phase boundaries are within 0-40°C according to previous studies.[32,34] We therefore set the dual Peltier stages at 40°C on the inlet side (corresponding to homogeneous L_1 micellar) and 0°C on the outlet side (mixed L_1+L_α(MLV) phase) and creating a thermal gradient along the microchannel spanning these values. The temperature of the microfluidic system is allowed to reach steady state before phase mapping.

The withdrawal flow rate sets both the timescale of the measurement of phase change and the temperature profile (cooling ramp) experienced by the fluid during convection across the microfluidic system. Typically, a value of 5 μL/min (detailed in the next section) is employed, in order to exceed the intrinsic timescales associated with the instability and its optical detection ($\simeq$150 s for this system). Further, possible device contamination from the analysis of multiple samples of distinct composition must be considered, and is largely mitigated by three steps in sample loading. By segmenting the flow, sample plugs are sequentially loaded with air plugs, cross-contamination is minimised; a wash step (with a miscible fluid, such as pure water, or an immiscible 'displacement' fluid) is also assessed; finally, surfactant samples are loaded into the microchannel in increasing order of concentration. The relative efficiency of these protocols is examined below.

Images of the microchannel at the temperature gradient were captured at an integration time of 10 ms in optical reflection mode, as a function of composition and flow rate, and batch processed in ImageJ to determine the light intensity profile along the channel direction. Images were first split into 2048 columns (normal to flow direction) and the average light intensity of each column was automatically computed. The phase transition from the micellar L_1 to the lamellar MLV phase results in a measurable reduction in light intensity, from which the location (and corresponding temperature) of the phase transition can be obtained. We define a variation of light intensity greater than 2 % between consecutive columns to signify the onset of phase change. Relative light intensities were computed pixel by pixel as $I_{rel.} = I/I_{clear}$ where I_{clear} is the light intensity of the sample in the micellar (homogeneous) solution.

IV. RESULTS AND DISCUSSION

A. Identification of phase boundary

The micellar to lamellar phase transition of NaLAS aqueous solutions (<30 wt%) results in the formation of micron sized multilamellar vesicles (MLVs) that coalesce and appear as darker features in optical microscopy. Detection of phase change can thus be carried out by the identification of sparse particle-like features in the microchannel. Representative images of the phase change location of five different NaLAS solutions, from 22.5% to 24.5% in increments of 0.5%, are presented in the Fig. 4. By contrast with bulk transitions, these nucleation events have low density and yield a mixed MLV-micellar phase with prescribed fractions. The microchannel position (x, indicated below) corresponds to a specific temperature (indicated above), as detailed in Fig. 3 based on experimental and simulation results. The location where phase change is first observed evidently varies with composition. Significantly, a relatively high optical magnification is required for their accurate detection, and therefore phase boundaries cannot be correctly identified using a wide field of view, low magnification optical (e.g. imaging) system. Microchannel position, illumination and imaging settings are kept constant during an experiment to enable correct background subtraction and reduce noise during image analysis. The quantitative analysis of the optical data shown in Fig. 4, is presented in Fig. 5(a) where the light intensity profile along the channel is plotted for five NaLAS aqueous solutions. To improve statistics data are averaged vertically, normal to channel position (i.e. along the y-direction) and normalized to 100% relative intensity, corresponding to the

transparent micellar phase. The position x where the reflected intensity drops (corresponding to MLV-formation) indicates the *apparent* phase boundary, at the measurement time and flow rate. Our system provides a direct correspondence between position and temperature, as shown in the top and bottom axis of Fig. 5(a,b). These measurements can then be readily plotted to define the boundary between the isotropic micellar phase (one phase region) and the lamellar phase (two phase region), as shown in Fig. 5(b). Upon decreasing surfactant concentration, the fraction of MLVs decreases and the detection of phase change becomes increasingly challenging. With the current optical system, NaLAS solution concentrations down to 10% and $\simeq$4°C could be readily analysed yielding $\lesssim$0.5% apparent MLV volume fraction, or projected area fraction, as shown in Supporting Information Fig. S1.

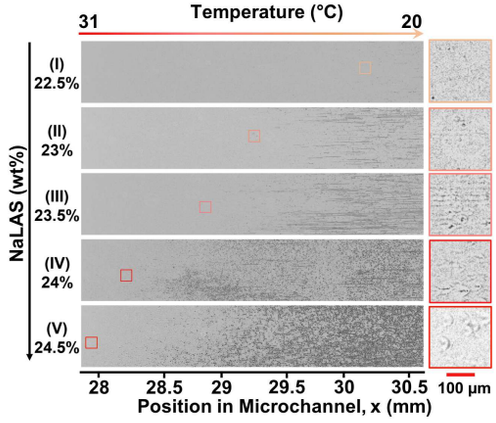

FIG. 4. Optical images of the phase change locations of selected NaLAS aqueous solutions of different concentrations sequentially loaded into the microchannel, along the thermal gradient at a flow rate of 5 μL/min. The images were background-subtracted and processed by ImageJ. The images in the coloured square boxes on the right side correspond to higher magnifications of the squares with the same color on the left side, where the phase transition is first detected. The correspondence between position along the microchannel and temperature is given in Fig. 3.

The accurate detection of phase change of the surfactant solution upon cooling takes place after a finite time, as illustrated in Fig. 6. Since the microfluidic system is thermally equilibrated and the sample equilibration time within the microchannel is very short (with respect to the flow velocity), the sample can be considered to be thermalized with the device ($<$1 s estimated from the thermal offset). This timescale is instead associated with the intrinsic kinetics of the micellar-to-MLV transformation and the time required for the liquid crystalline surfactant assemblies to grow to optically detectable dimensions ($>1\mu$m) and with sufficient number density. The relative light intensity of a 24 wt% LAS solution over different time scales at a low flow rate (1 μL/min) is plotted in Fig. 6(a). The time of the first appearance of MLVs (and thus initial phase change) after the introduction of the sample in the microchannel is selected as time t=0 s; thereafter, the *apparent* location of the phase transition evolves with elapsed time.

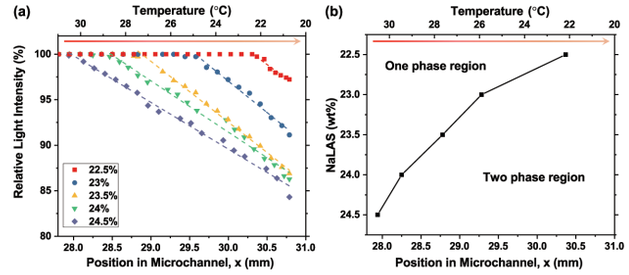

FIG. 5. (a) Relative light intensity variation along channel position (and corresponding temperature) for NaLAS aqueous solutions of 22.5-24.5 wt%. The intensity remains highest in the micellar (one-phase) region before decreasing at the apparent phase change temperature. Symbol and line colours correspond to the coloured square boxes in Fig. 4. (b) Location and temperature where the phase change is detected, obtained from (a), found to increase with surfactant concentration as expected.

The phase change position appears initially at a low temperature ($\simeq$27.5 °C, t=1 s) and shifts towards the inlet side (higher temperature) before reaching a time-invariant (or steady-state) location along the channel position corresponding to $\simeq$29.5 °C after approximately t=150 s. This time scale is also illustrated in the measurement of the relative light intensity at a fixed location in the microchannel shown in Fig. 6(b). For this surfactant system, we find that each concentration must be loaded for $\simeq$2.5 min to observe a stable phase transition temperature (and a modest $\sim$ 2°C is apparent after t=1 s of introducing the sample at this concentration and flow rate, shown by the red data set in Fig 6(a)).

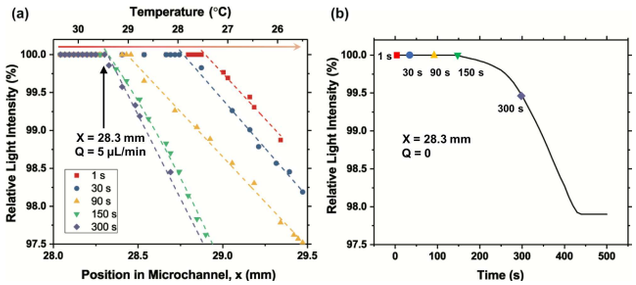

FIG. 6. (a) Temporal evolution of relative light intensity of a 24 wt% surfactant concentration along the microchannel, after first detection of phase change at flow rate of Q=5 μL/min, indicated by the red data set. The phase change location evolves with time before reaching a static position after 150 s (discussed in the text). (b) Quiescent measurement (i.e., in the absence of flow) of the relative light intensity at a reference phase change location (x=28.3 mm) over time. The intensity starts to decrease at 150 s which corresponds to the time scale measured in (a), associated with MLV formation under these conditions and the finite spatial resolution and contrast of the setup.

B. Metastable zone width

We next explore the role of the flow rate and direction of the thermal gradient in the detection of phase change. In particu-

lar, we consider its effect in the reversibility of the transition as a means to develop a facile MSZW estimation. Conceptually, an 'excessively large' flow rate should not allow adequate thermalization of the sample with the imposed thermal gradient, while an 'excessively low' flow rate might enable thermal diffusion and the smearing of the detection of phase change. As shown in Fig. 7, the relative light intensity of 24 wt% LAS is plotted for different flow rates in the microchannel. For comparison, we include a quiescent experiment (i.e. in the absence of flow, labelled as '0 μL/min'). This experiment was carried out in the microchannel setup by injecting the sample in the micellar phase, with both Peltier modules set to $T_1 = T_2$=40°C, stopping the flow, and then equilibrating T_2 gradually to 0°C to yield the stepped temperature profile. This dataset trace is included in Fig. 7 as an 'equilibrium' reference. As the flow rate decreases from 15 μL/min, the We find that the phase change position moves towards the inlet (lower position x, and higher temperatures). The temperature profile in the microchannel also shifts, albeit only marginally at these flow rates, as shown in Fig. 3. At or below 5 μL/min, we find that the optical detection of phase change to yield invariant temperature values. It takes $\simeq$15 s for a fluid element to travel across the observation window at 5 μL/min, enabling reliable measurements of the transition, while higher flow rates require shorter image integration times. For the current system, we find a flow rate of 5 μL/min to provide a suitable compromise between measurement speed and accuracy.

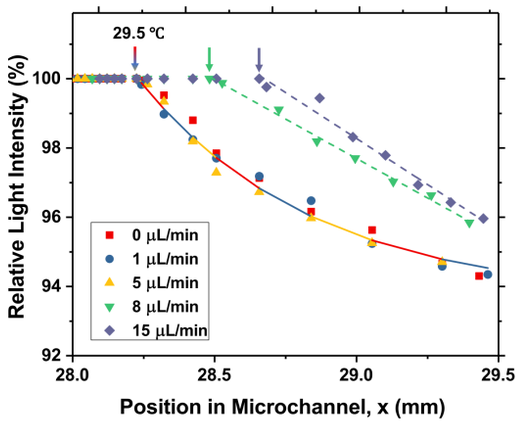

FIG. 7. Relative light intensity of 24 wt% NaLAS sample flowing at different flow rate (indicated) along the microchannel. The phase change location (and thus temperature) is unchanged for the lower flow rate ($\leq$5μL/min) and moves toward the colder direction at higher flow rate. The temperature profile does not change appreciably for these rates, as shown in Fig. 3.

The asymmetry of the phase change temperatures upon heating and cooling results in the metastable zone width (MSZW) for these surfactant solutions, whose value is rate dependent and of great practical importance,[35] often measured by the so-called 'polythermal' method. In our system, cooling (or heating) rate, $\Delta T/\Delta t$, is dictated by the temperature difference between the thermal stages and the flow rate of the

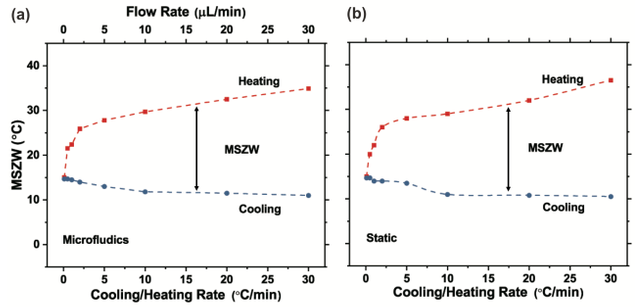

FIG. 8. Metastable zone width (MSZW) determination for a 20 wt% NaLAS solution measured by the (a) microfluidic and (b) conventional static method, as a function of cooling/heating rate. The blue line marks the appearance of MLVs from the micellar phase upon cooling (in microfluidics, corresponding to flowing from high to low temperature), while the red line indicates complete dissolution of L_α back to micellar phase (from low to high temperature). The microfluidic heating/cooling rate are set by the temperature difference between two stages and flow rate.

sample. Specifically, it is product of two terms: (i) the temperature difference between hot and cold stages $\Delta T/\Delta x$ and (ii) the flow rate that subsequently determines the fluid velocity $\Delta x/\Delta t = Q/A$, where Q is flow rate and A the cross-sectional area of the channel, assuming plug flow. We thus obtain $\Delta T/\Delta t = (\Delta T/\Delta x) \times (\Delta x/\Delta t)$. For a fixed ΔT, increasing Q increases the cooling/heating rate and thus changes the apparent MSZW. To expedite MSZW measurement, we employ a U-shaped microchannel, illustrated in Fig. 2(a). Keeping the dual temperature stage at 40/0°C, we investigate a 20 wt% NaLAS under this configuration by varying Q, whose results are shown in Fig. 8(a). The blue line represents the change from micellar L_1 to MLV lamellar L_α phase as the solution is convected from high to low temperature, while the red line indicates the reverse trajectory. When the solution travels from high to low temperature, Fig. 7 exhibits the same critical flow rate as in Fig. 6. At higher flow rate ($>$5 μL/min), and thus higher cooling/heating rate, the apparent MSZW becomes wider. A quiescent measurement of MSZW carried out on the same LAS solution (by placing the sample within a glass cuvette) and the results are shown in Fig. 8(b). The solution is cooled/heated at comparable rates as in the microfluidic platform and observed under the microscope. The overall profile coincides for both methods, showing qualitative and quantitative agreement for the dynamic (microfluidic) and static polythermal MSZW measurement, however the measurement time is considerably shorter in the former. The total polythermal measurement time using the reversible microfluidic chip is $<$2 h for all rates, while the conventional method requires $>$10 h.

C. Validation with Optical and SANS measurements

In this section, we compare experimental results obtained with the microfluidic platform with those obtained by static

microscopy and small-angle neutron scattering (SANS) measurements. The static measurements are performed as described in Fig. 1.

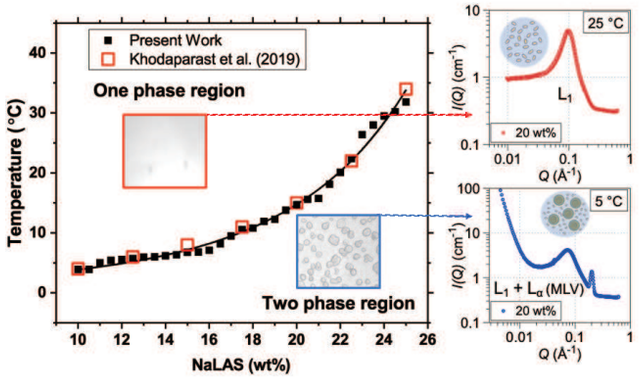

FIG. 9. Phase diagram of LAS/H_2O micellar solutions, within 10-25% surfactant, mapped with current microfluidic setup (■) compared with static optical microscopy (red □).[32] At high temperatures, optically transparent solutions comprise ≃3 nm ellipsoidal micelles, as seen by SANS at 25°C (red data, L_1). Upon cooling (5°C shown), MLVs form and coexist with the micellar phase, inferred from blue SANS data, with a Bragg peak ($Q \simeq 0.2$ Å^{-1}), corresponding to the spacing between lamellar L_α sheets (≃ 3 nm), and scattering upturn from the overall MLV.

A phase diagram of NaLAS/water is plotted with 32 weight concentrations over a 10-25 wt% concentration range (below L_α formation at ambient conditions) using current setup in Fig. 9. The phase boundaries are obtained for cooling cycles performed at the minimum rates of cooling (0.1 °C/min) and shown by full black squares. Comparison with previous work[32] (open red squares) by quiescent microscopy and SANS provides robust validation of the method and similar precision (≃1°C). Optical microscopy images illustrate the (isotropic) micellar and MLV lamellar phase at long times, accompanied by static SANS measurements at 25 °C and 5 °C.

Employing conventional approaches, each solution at one concentration is cooled down at a relatively low rate to locate the phase change temperature. For instance, to investigate a temperature range between 40 to 0 °C at a cooling rate of 0.1 °C/min requires in excess of 6 h. Often this delay is mitigated by simultaneously imaging several, however, relatively high optical resolution is needed to resolve nucleation events or low demixed volume fractions, and thus sequential measurements are required. With the current method, as different solution concentrations travel within the microchannel subjected to a stationary thermal field, measurement times can be significantly reduced without compromising accuracy. The aspirated sample volume must be sufficient to enable a steady state measurement, but generally does not have to exceed an entire channel length, such that several samples can be simultaneously present within a channel, segmented with an immiscible fluid (or gas, such as air, or an inert gas). The sample plug length and flow rate effectively define the time available for measurement, thereby placing an upper cap on the flow rate during measurement. During the sample loading (and possibly cleaning) step, however, this cap can be significantly relaxed and much faster rates employed. Fig. 10 illustrates various possible operation modes. We indicate the sample injection in 'green', whose maximum flow rate is effectively determined by the necessary residence time in the microchannel to detect the instability; the flow rate of the cleaning fluid, water in the present case, is shown in 'blue', and can be much greater than that of the sample injection; further, sample loading into the chip can also be faster, prior to measurement. Under typical measurement conditions (of viscosity and channel geometry), the maximum flow rate is not limited by device hydrodynamic resistance. When swapping inputs between different samples, or cleaning fluid, a short air plug (shown in white) is also inserted in the fluid sequence. Fig. 10(a,b,c) illustrates the variation of measurement cycle time at fixed flow rates 5 μL/min for sample measurement and 500 μL/min for the cleaning (and loading). For instance, in Fig. 10(b), a single measurement of one concentration takes ≃5 min when 50% of the channel is filled with the solution (12 μL) at the flow rate of 5 μL/min, and thus ≃150 min to examine more than 30 concentration points. Fig. 10(d) shows the coupling between sample volume, measurement time, and cycle frequency at three representative flow rates. Further to reducing sample measurement cycle time, considerable paralellization of measurements is evidently possible by introducing additional channels (10-100) within the same microdevice.

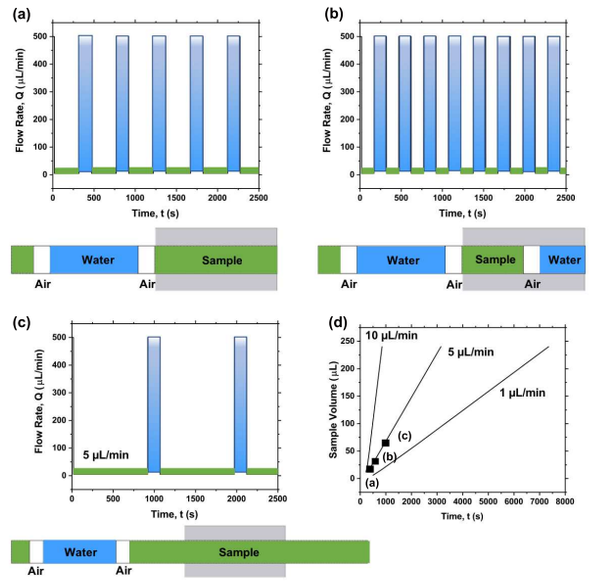

FIG. 10. Illustration of relative timescales associated with sampling volume and sampling protocol. The entire microchannel length (60 mm) is indicated by the gray area. (a) 100% of the channel is filled with solution, (b) 50% of the channel is filled with solution, (c) 3× the channel length is filled with solution. The flow rates in the illustration are $Q = 5$ μL/min during measurement and $Q = 500$ μL/min during sample loading and cleaning procedure. (d) The relation between volume of a single sample and the sample loading and cleaning time with flow rate for protocols (a)-(c).

D. Reproducibility, cleaning and contamination

To examine the suitability of flow segmentation with air plugs (introduced between sampling of distinct compositions) in compartmentalizing individual samples, we run a series of measurements of the same sample concentration in alternating order, as shown in Fig. 11. The first series of measurement take place in increasing concentrations (from low to high NaLAS content), while three selected measurements take place in alternating order. The phase change temperature of the different runs varies by no more than 0.5°C, in line with the reproducibility of static measurements. We therefore conclude that introducing an air plug provides an adequate strategy for isolating different sample compositions of this system. However, a washing step can be trivially incorporated in this work process (detailed in Supporting Information).

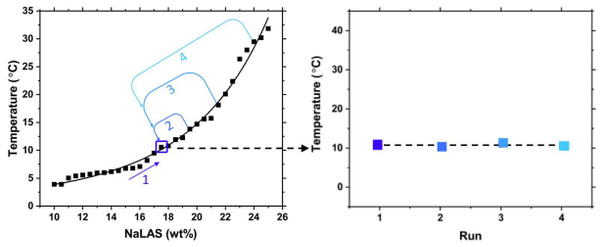

FIG. 11. Comparison of the phase change temperature for a sample of the same concentration (17.5 wt% NaLAS) measured in increasing and alternating order of concentration. The first run is measured in increasing order of concentration, while selected repeated measurements take place in different order, indicated by the blue arrows. All measurements were carried out at a flow rate $Q = 1$ μL/min and temperature stages set at 40 and 0 °C. Repeated measurements exhibit consistent results, indicating that the segmented flow approach is effective in mitigating cross-contamination.

V. CONCLUSION

We present a microfluidic platform for rapid phase mapping of liquid formulations (illustrated here with a surfactant solution) employing a multiwell plate sample library and the sequential loading of segmented samples across a stationary temperature profile. The platform automatically withdraws samples from the multiwell plate employing an xy stage and z-actuator connected to a needle tubing connected to a syringe pump via a microfluidic chip. The chip is placed into a prescribed temperature profile which, together with the withdrawal flow rate, defines the spatial-temporal temperature profile. A commonly employed biodegradable surfactant NaLAS in aqueous solution was employed in the evaluation of the platform. We report various phase mapping protocols and discuss the implications of measurement time required to observe phase changes (with intrinsic thermodynamic and kinetic properties) and flow rate, as well as temperature gradient. Under the established operating conditions, the platform yields accurate phase behaviour measurements, validated by conventional methods, but with increased speed without compromising on accuracy. By employing segmented, continuous microchannel flow, the phase change position could be precisely located spatially along the microdevice, which can then be mapped onto a temperature scale yielding a steady-state phase transition image. The system could map NaLAS/water mixtures between 10-25 wt% in ∼3 h unattended. By employing U-shaped microchannels, the platform could directly probe the reversibility of a phase change by thermal cycling. We demonstrate that such configuration provides facile MSZW measurements by the polythermal method in shortened timescales by simply varying flow rate. Finally, parallelization of the system is possible by placing multiple channels side by side along the same thermal profile and operated by a manifold of liquid withdrawal systems, which can be useful to further expedite measurement, explore wider composition phase spaces, or acquire statistics on, for instance, activated processes such as demixing or crystallisation by nucleation and growth.

VI. SUPPLEMENTARY MATERIAL

The supplementary material contains the data and discussion of phase change identification at lower surfactant concentration and the cleaning between different concentrations of solution.

ACKNOWLEDGMENTS

The authors acknowledge the financial support of the National Formulation Centre (NFC) of the Centre for Process Innovation (CPI), Procter & Gamble and BP-Castrol and the microSTAR project team.

[1]T. Hargreaves, *Chemical Formulation - An Overview of Surfactant-Based Preparations Used in Everyday Life* (Royal Society of Chemistry, 2003).
[2]R. G. Laughlin, *The aqueous phase behavior of surfactants* (London : Academic, c1994).
[3]T. F. Tadros, *Applied surfactants : principles and applications* (Wiley-VCH, 2005).
[4]J. L. Jones and T. C. B. McLeish, "Rheological response of surfactant cubic phases," Langmuir **11**, 785–792 (1995).
[5]D. Myers, *Surfactant Science and Technology* (Wiley, 2005).
[6]I. Johansson and P. Somasundaran, *Handbook for Cleaning/Decontamination of Surfaces* (Elsevier, 2007).
[7]J. T. Cabral and A. Karim, "Discrete combinatorial investigation of polymer mixture phase boundaries," Measurement Science and Technology **16**, 191–198 (2004).
[8]J. Wang, D. R. Hallinger, A. S. Murr, A. R. Buckalew, R. R. Lougee, A. M. Richard, S. C. Laws, and T. E. Stoker, "High-throughput screening and chemotype-enrichment analysis of toxcast phase ii chemicals evaluated for human sodium-iodide symporter (nis) inhibition," Environment international **126**, 377–386 (2019).
[9]P. Kheddo, J. E. Bramham, R. J. Dearman, S. Uddin, C. F. van der Walle, and A. P. Golovanov, "Investigating liquid–liquid phase separation of a monoclonal antibody using solution-state nmr spectroscopy: Effect of arg·glu and arg· hcl," Molecular pharmaceutics **14**, 2852–2860 (2017).
[10]L. Gan, M. Zhou, D. Yang, and X. Qiu, "Preparation and evaluation of carboxymethylated lignin as dispersant for aqueous graphite suspension using turbiscan lab analyzer," Journal of Dispersion Science and Technology **34**, 644–650 (2013).

[11]J. Liu, X.-f. Huang, L.-j. Lu, M.-x. Li, J.-c. Xu, and H.-p. Deng, "Turbiscan lab® expert analysis of the biological demulsification of a water-in-oil emulsion by two biodemulsifiers," Journal of hazardous materials **190**, 214–221 (2011).

[12]D. J. Mcclements, "Critical review of techniques and methodologies for characterization of emulsion stability," Critical Reviews in Food Science and Nutrition **47**, 611–649 (2007).

[13]D. Lerche and T. Sobisch, "Direct and accelerated characterization of formulation stability," Journal of Dispersion Science and Technology **32**, 1799–1811 (2011).

[14]O. Mengual, G. Meunier, I. Cayre, K. Puech, and P. Snabre, "TURBISCAN MA 2000: multiple light scattering measurement for concentrated emulsion and suspension instability analysis," TALANTA **50**, 445–456 (1999), Symposium on Analytical Sciences (6th SAS), VALENCIA, SPAIN, JUN 22-24, 1998.

[15]B. Skolova, K. Hudska, P. Pullmannova, A. Kovacik, K. Palat, J. Roh, J. Fleddermann, I. Estrela-Lopis, and K. Vavrova, "Different phase behavior and packing of ceramides with long (c16) and very long (c24) acyls in model membranes: infrared spectroscopy using deuterated lipids," The Journal of Physical Chemistry B **118**, 10460–10470 (2014).

[16]W. Kong, S. Li, H. Ke, H. Zhang, and J. Baeyens, "The use of ultrasound probes to monitor multi-phase behavior in opaque systems," Particuology **45**, 91–97 (2019).

[17]V. E. Blair, K. Celebi, K. Müllen, and J. Vermant, "Electrically conductive thin films derived from bulk graphite and liquid–liquid interface assembly," Advanced Materials Interfaces **6**, 1801570 (2019).

[18]G. M. Whitesides, "The origins and the future of microfluidics," Nature **442**, 368 (2006).

[19]T. M. Squires and S. R. Quake, "Microfluidics: Fluid physics at the nanoliter scale," Reviews of modern physics **77**, 977 (2005).

[20]Y. Shangguan, D. Guo, H. Feng, Y. Li, X. Gong, Q. Chen, B. Zheng, and C. Wu, "Mapping phase diagrams of polymer solutions by a combination of microfluidic solution droplets and laser light-scattering detection," Macromolecules **47**, 2496–2502 (2014).

[21]P. Laval, N. Lisai, J.-B. Salmon, and M. Joanicot, "A microfluidic device based on droplet storage for screening solubility diagrams," Lab Chip **7**, 829–834 (2007).

[22]J. Shim, G. Cristobal, D. R. Link, T. Thorsen, Y. Jia, K. Piattelli, and S. Fraden, "Control and measurement of the phase behavior of aqueous solutions using microfluidics," Journal of the American Chemical Society. **129**, 8825–8835 (2007).

[23]J. Leng, M. Joanicot, and A. Ajdari, "Microfluidic exploration of the phase diagram of a surfactant/water binary system," Langmuir **23**, 2315–2317 (2007).

[24]S. D. Hudson, F. R. Phelan, M. D. Handler, J. T. Cabral, K. B. Migler, and E. J. Amis, "Microfluidic analog of the four-roll mill," Applied Physics Letters **85**, 335–337 (2004).

[25]L. Zhang, E. N. Wang, K. E. Goodson, and T. W. Kenny, "Phase change phenomena in silicon microchannels," International Journal of Heat and Mass Transfer **48**, 1572 – 1582 (2005).

[26]A. S. Poulos, M. Nania, P. Lapham, R. M. Miller, A. J. Smith, H. Tantawy, J. Caragay, J. Gummel, O. Ces, E. S. J. Robles, and J. T. Cabral, "Microfluidic saxs study of lamellar and multilamellar vesicle phases of linear sodium alkylbenzenesulfonate surfactant with intrinsic isomeric distribution," Langmuir **32**, 5852–5861 (2016), pMID: 27196820.

[27]M. Adamo, A. S. Poulos, R. M. Miller, C. G. Lopez, A. Martel, L. Porcar, and J. T. Cabral, "Rapid contrast matching by microfluidic sans," Lab Chip **17**, 1559–1569 (2017).

[28]H. P. Martin, N. J. Brooks, J. M. Seddon, P. F. Luckham, N. J. Terrill, A. J. Kowalski, and J. T. Cabral, "Microfluidic processing of concentrated surfactant mixtures: online saxs, microscopy and rheology," Soft Matter **12**, 1750–1758 (2016).

[29]M. U. Kopp, A. J. De Mello, and A. Manz, "Chemical amplification: continuous-flow pcr on a chip," Science **280**, 1046–1048 (1998).

[30]C. D. Ahrberg, A. Manz, and B. G. Chung, "Polymerase chain reaction in microfluidic devices," Lab on a Chip **16**, 3866–3884 (2016).

[31]J. J. Scheibel, "The evolution of anionic surfactant technology to meet the requirements of the laundry detergent industry," J. Surfactants Deterg. **7**, 319–328 (2004).

[32]S. Khodaparast, W. Sharratt, H. Wang, E. S. Robles, R. Dalgliesh, and J. T. Cabral, "Spontaneous formation of multilamellar vesicles from aqueous micellar solutions of sodium linear alkylbenzene sulfonate (nalas)," Journal of Colloid and Interface Science **546**, 221 – 230 (2019).

[33]J. T. Cabral, S. D. Hudson, C. Harrison, and J. F. Douglas, "Frontal photopolymerization for microfluidic applications," Langmuir **20**, 10020–10029 (2004).

[34]J. A. Stewart, A. Saiani, A. Bayly, and G. J. T. Tiddy, Colloids Surf., A **338**, 155–161 (2009).

[35]R. M. Miller, O. Ces, N. J. Brooks, E. S. J. Robles, and J. T. Cabral, "Crystallization of sodium dodecyl sulfate-water micellar solutions under linear cooling," *Crystal Growth & Design*, Crystal Growth & Design **17**, 2428–2437 (2017).

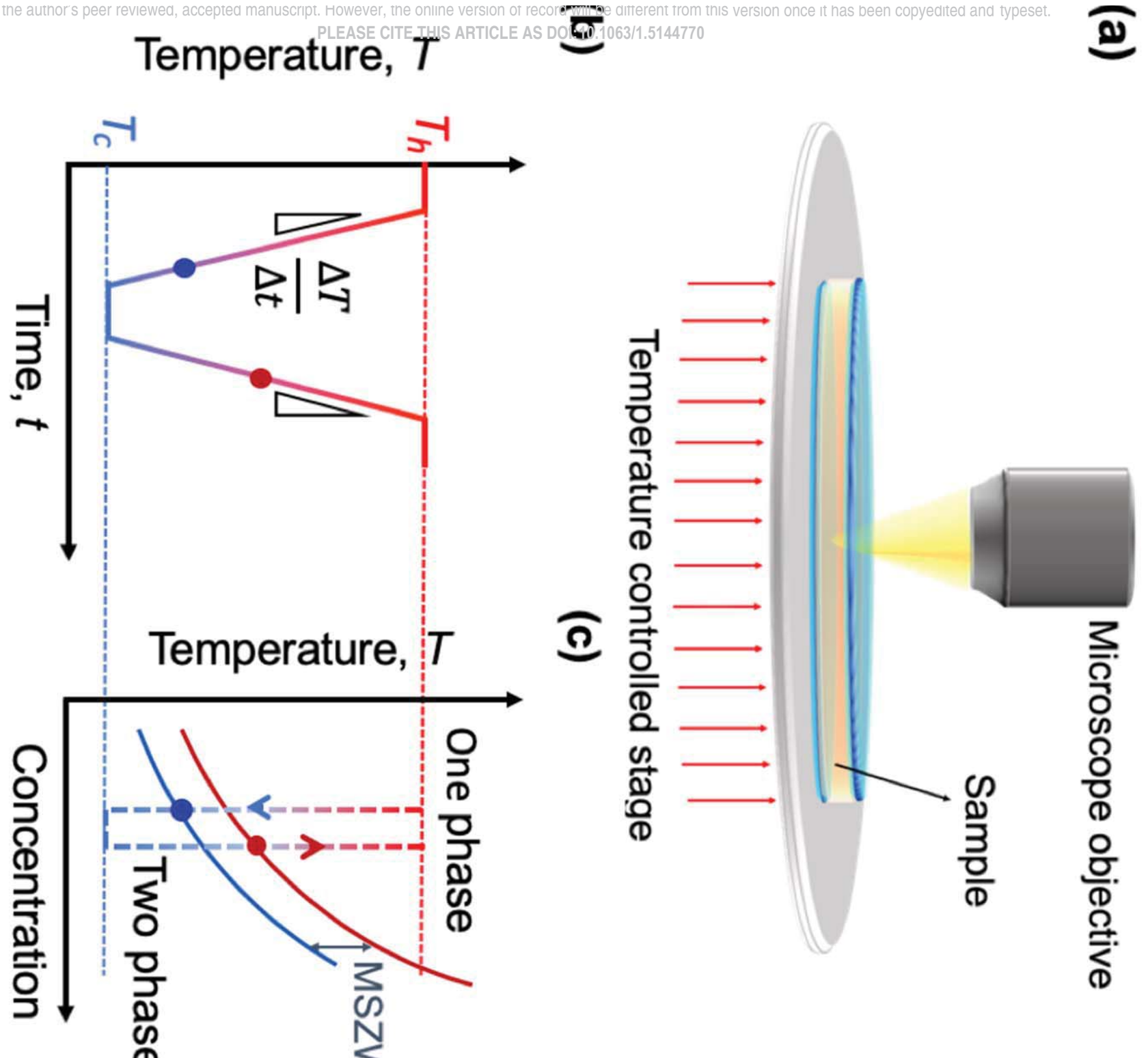

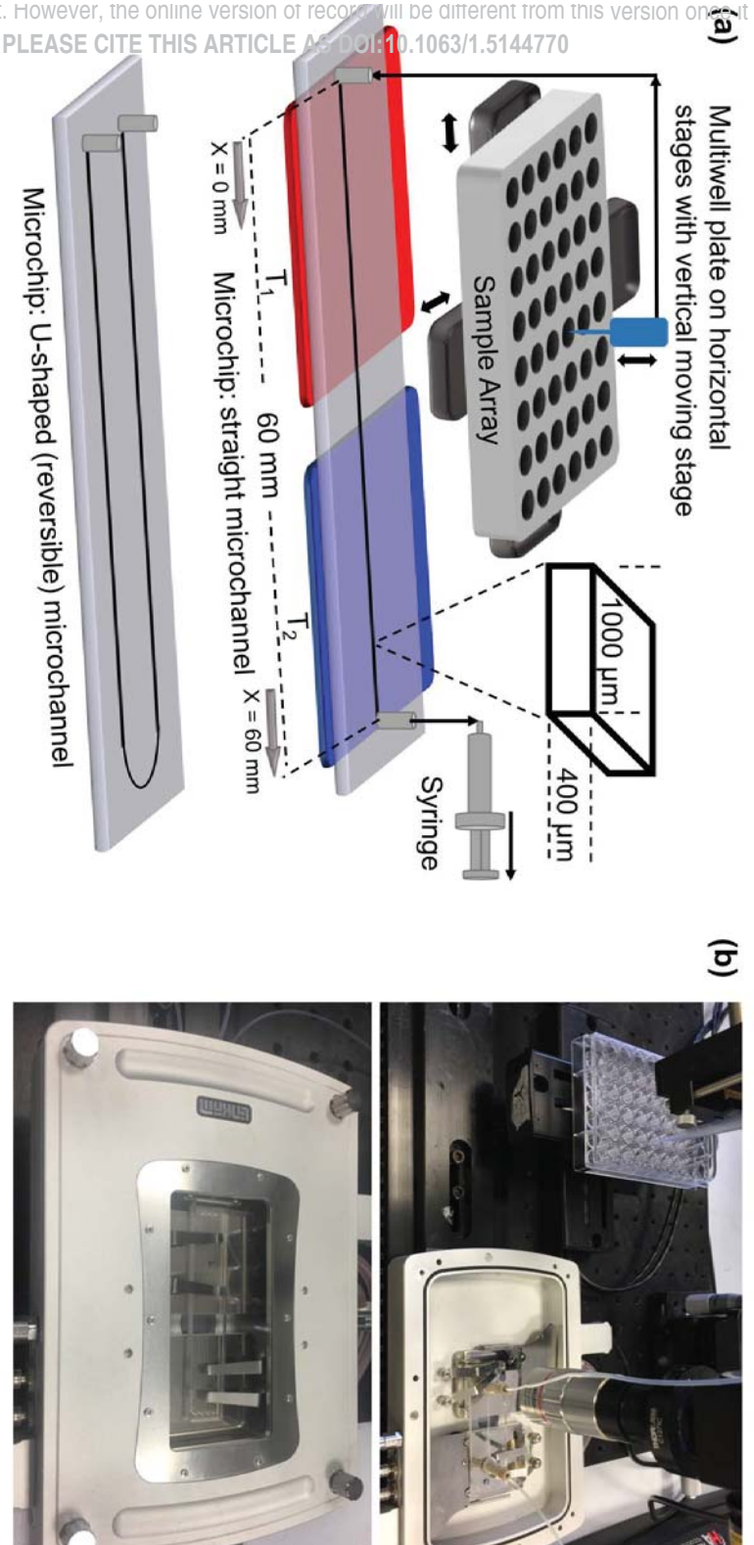

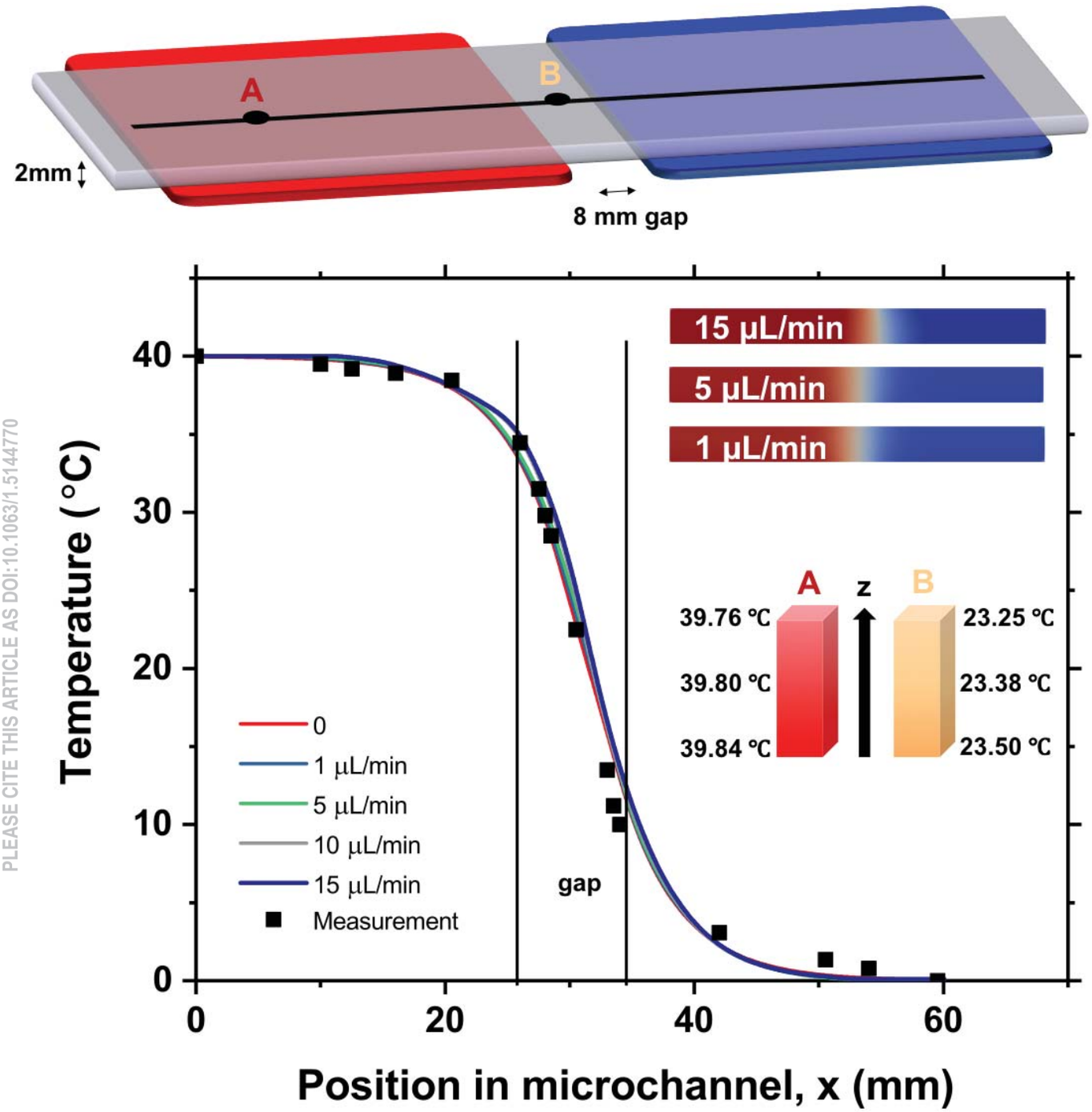

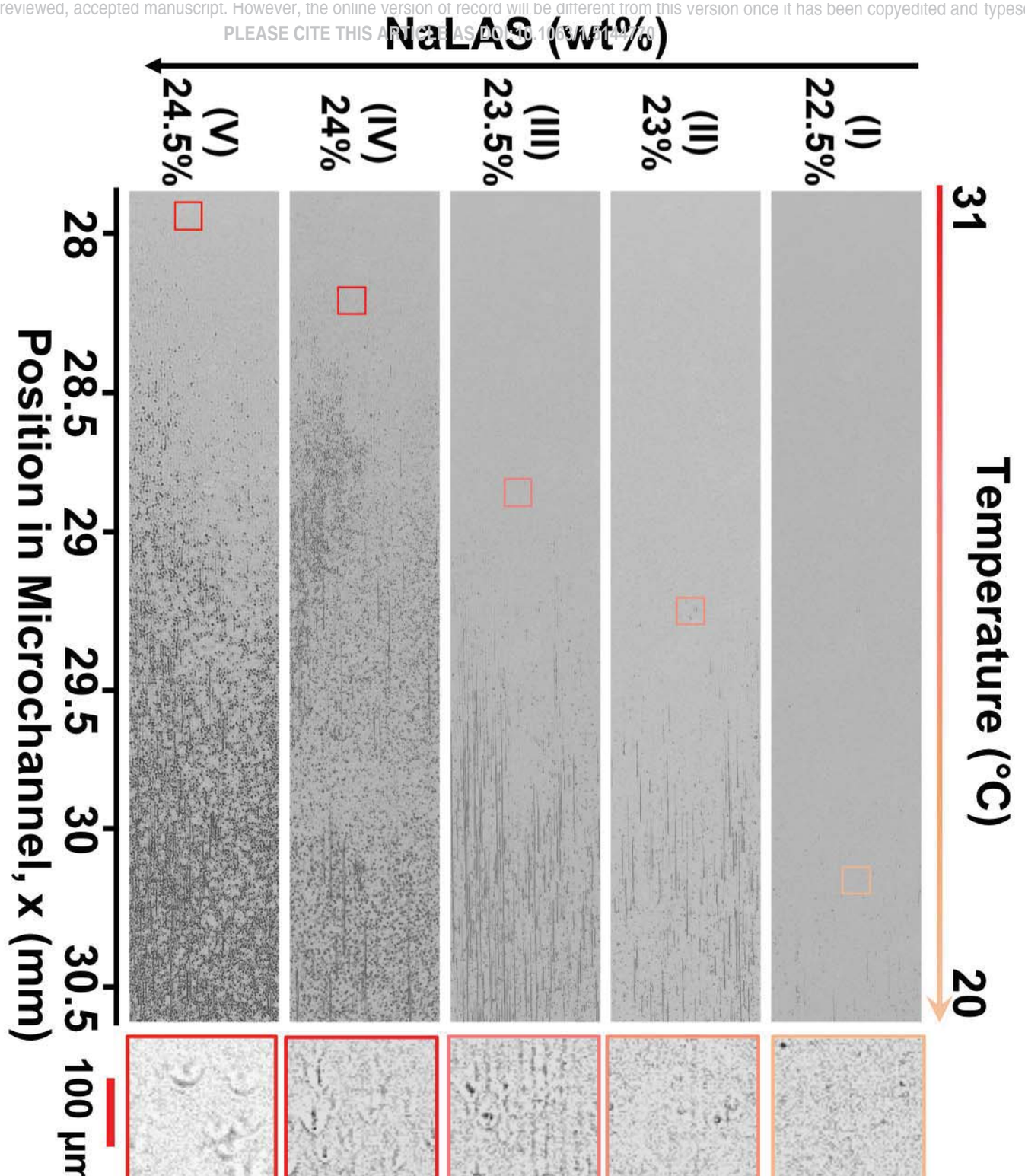

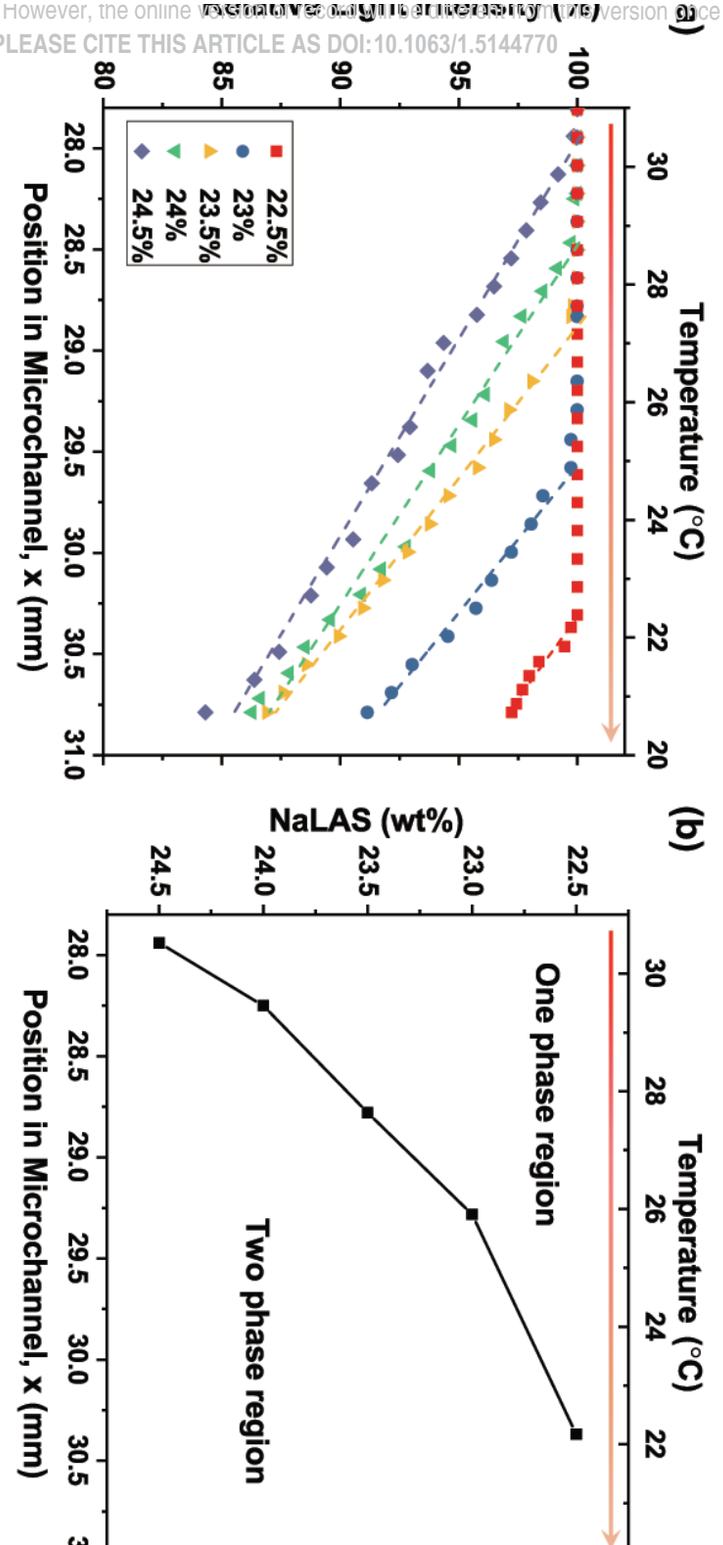

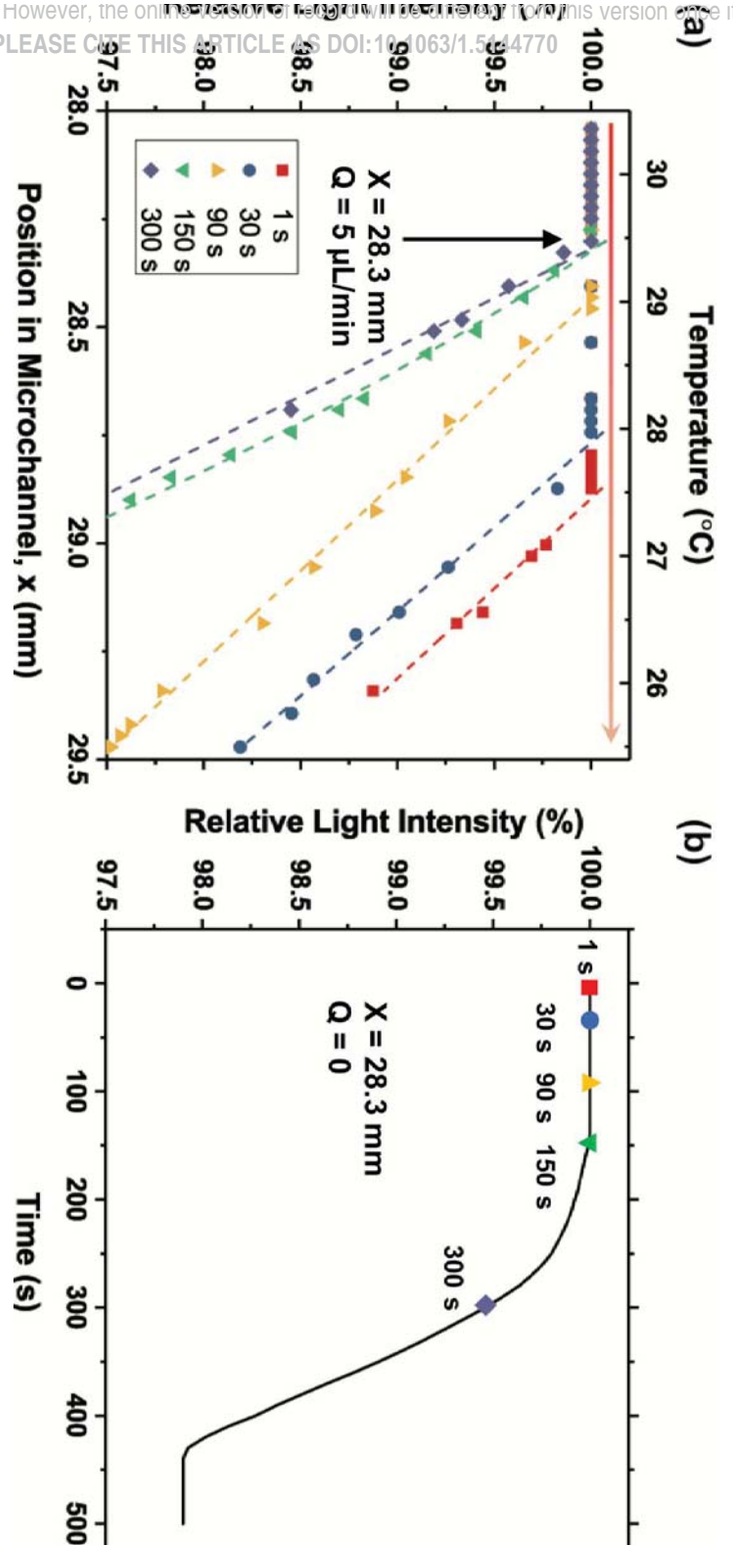

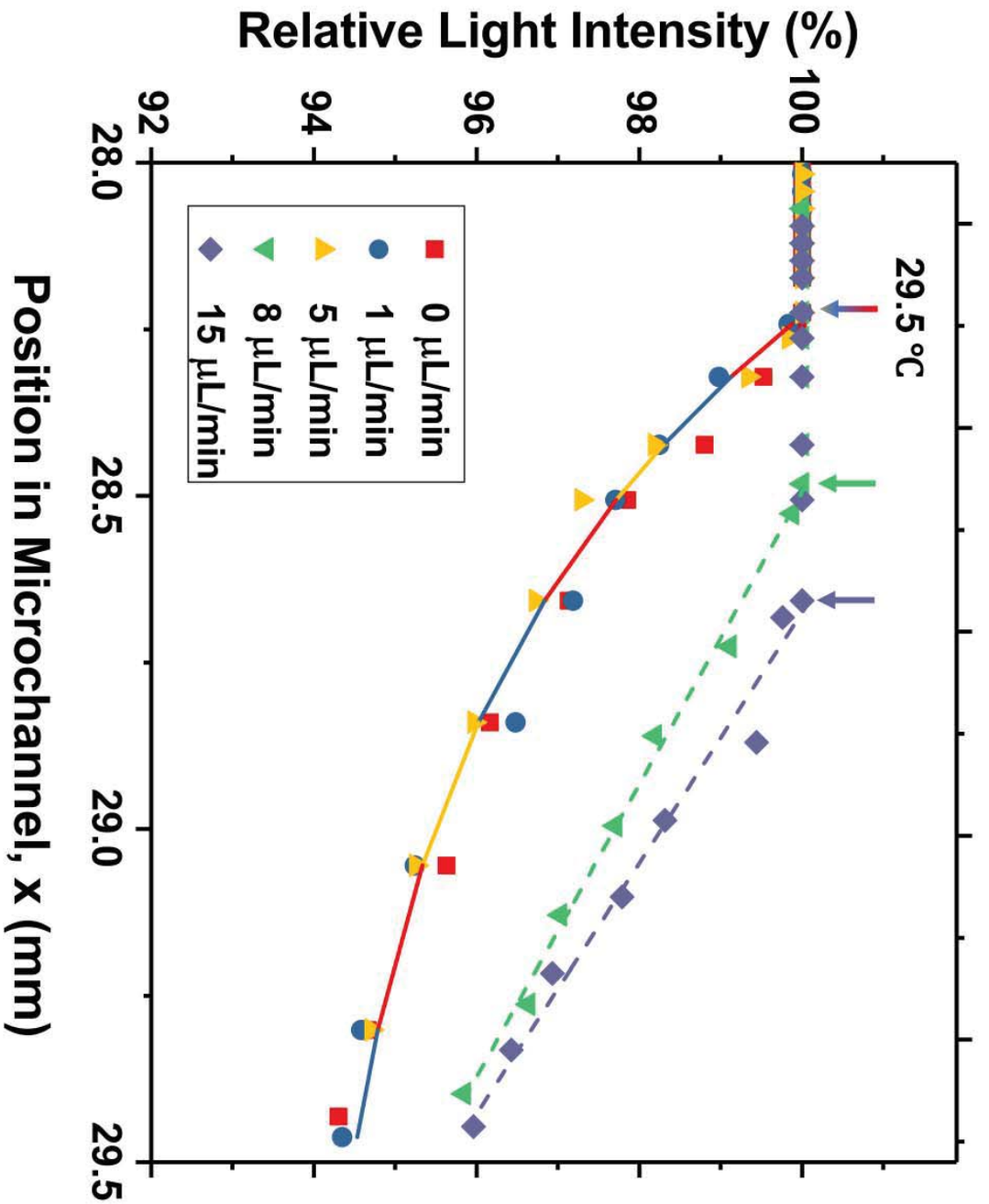

Review of Scientific Instruments